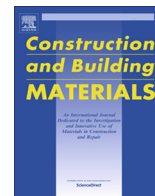




Contents lists available at ScienceDirect

# Construction and Building Materials

journal homepage: [www.elsevier.com/locate/conbuildmat](http://www.elsevier.com/locate/conbuildmat)

## A novel rapid microwave-thermal process for accelerated curing of concrete: Prototype design, optimal process and experimental investigations



Phadungsak Rattanadecho<sup>a,\*</sup>, Natt Makul<sup>b</sup>, Aumpol Pichaicherd<sup>a</sup>, Porncharoen Chanamai<sup>a</sup>, Bunyong Rungroungdouyboon<sup>a</sup>

<sup>a</sup> Center of Excellence in Electromagnetic Energy Utilization in Engineering (CEEE), Department of Mechanical Engineering, Faculty of Engineering, Thammasat University Pratum Thani, 12121, Thailand

<sup>b</sup> Building Technology Program, Faculty of Industrial Technology, Phranakhon Rajabhat University, 3 Moo 6 Changwattane Road, Anusaowari Sub District, Bang Khen District, Bangkok 10220, Thailand

### HIGHLIGHTS

- Novel rapid microwave-thermal process for accelerated curing of concrete.
- MW at an operating frequency of 2.45 GHz and at powers of 400 W and 800 W.
- A mobile microwave (MW)-assisted curing unit was designed.
- Mathematical models were applied to design a horn-shaped MW cavity.
- MW energizing for 15 min/time and a paused duration of 60 min were included.

### ARTICLE INFO

#### Article history:

Received 14 December 2015

Received in revised form 14 July 2016

Accepted 15 July 2016

#### Keywords:

Concrete  
Heating  
Microwave technology  
Prototype  
Rapid thermal processing

### ABSTRACT

In this work, a mobile microwave (MW)-assisted curing unit for the accelerated curing of concrete workpiece is designed based on coupled electromagnetic (MW)-thermal analysis. The design of this unit is described together with experimental investigations into the heating characteristics of concrete workpiece subjected to the MW-accelerated curing process. Mathematical models are applied to design a horn-shaped MW cavity and as a basis for constructing a stationary and a moving MW-accelerated curing unit that uses MW energy at an operating frequency of  $2.45 \pm 0.05$  GHz and at powers of 400 W and 800 W. The experiments included the effects of MW curing on the temperature evolution, moisture content variation, and compressive strength development properties of the concrete. Also, the concrete workpiece was compared to water-cured conventional concretes and air-cured conventional concretes on the basis of these properties. Based on the concept of antenna, a rectangular horn-shaped cavity of 246.7 mm wide  $\times$  333.68 mm long is designed showing a uniform thermal distribution for concrete curing. From the experiments, it was found that the application period for curing using the mobile MW-curing unit was considerably shorter than for conventional curing methods. The appropriate pre-heating interval is 30 min, and MW energizing for 15 min/time and a paused duration of 60 min produces maximum compressive strength. However, the time needed for curing was considerable. When concrete was heated using MW energy for more than 90 min at over 80 °C, the effect was a continuous decrease in compressive strength. Further, at early age, the compressive strength development of the concrete workpiece subjected to MW curing was greater than that achieved by air curing or water wet-curing.

© 2016 Elsevier Ltd. All rights reserved.

### 1. Introduction

Microwave (MW)-assisted heating has emerged as an innovative and popular heating-process technology for dielectric

materials. A particularly efficient technique for thermal processes, MW-assisted heating can considerably reduce the time needed for heating/drying. A number of other analyses of the microwave heating process have appeared in the recent literature [1–4]. MW-assisted heating has been used successfully in numerous industrial processes, including the following:

\* Corresponding author.

E-mail address: [ratphadu@engr.tu.ac.th](mailto:ratphadu@engr.tu.ac.th) (P. Rattanadecho).

- Food and biological materials: Regier and Schubert [5] published a book in which they give an account of a wide range of microwave processing applications used worldwide including blanching, thawing, and packaging. Afrin et al. [6] investigated thermal lagging in living biological tissue and found that the phase lag times for temperature gradient and heat flux are indistinguishable in the respective cases of blood and tissue. Irishina et al. [7] studied a level set evolution strategy in microwave imaging for early breast cancer detection. Basak [8] studied thermal MW processing and concluded that it is an efficient way to produce a high temperature in a customized plane-wave oven.
- Wood: Perre and Turner [9] presented the effects of the combined convective and microwave drying of softwood by focusing on predicting the locations of hot spots and thermal runaway within the workpiece from the viewpoint of product quality. Kaensup et al. [10] used a combined microwave fluidized bed dryer to dry pepper seeds. The results indicated that MW energy dried the pepper seeds at a faster rate than a conventional fluidized bed did.
- Accelerated-curing and repairing of concrete: Leung and Pheeraphan [11] showed that MW energy can be used to cure concrete for practical construction applications. Makul et al. [12] used MW energy at an operating frequency of 2.45 GHz and a multi-mode cavity to cure early-stage Portland cement paste. Their research showed that based on steady heat transfer conduction the temperature increased consistently in accord with the mathematical model.

Up to the present time, the focus of research and development pertaining to the technology used to repair concrete has focused on reducing the time taken to complete repairs. However, the time needed to cure concrete is still lengthy and the process relies on conventional curing technology for repairs such as applying a curing compound, water ponding [13], and using a wetting sag to cover the concrete surface so that the concrete retains moisture content. This long period leads to problems; for example, when roads are repaired, traffic jams inevitably ensue as fewer lanes are available. Therefore, any method such as the use of streams or hot air with the potential to reduce the time needed in the initial concrete-curing phase is of great interest. However, these methods have the drawback of producing intermittent thermal distribution in concrete, leading to a reduction in compressive strength and causing the internal structure to break down [14]. Therefore, MW-heating technology applied to concrete curing in the initial phase is advantageous because heat can be produced in a way that is more efficient than with other methods.

It is well known that thermal-curing methods have an adverse effect on the properties of concrete—both at early age and in the long term. Therefore, a crucial question arises: Can the MW-heating method be applied in the concrete industry? Theoretically, it is possible. This is because materials used to make concrete, such as hydraulic Portland cement, aggregates, water, and admixtures are dielectric; i.e., they can absorb MW energy effectively. For example, Xuequan [15] proposed a new kind of MW-curing technique for concrete. Based on removing free water from the internal concrete's structure before any plastic shrinkage and loss of porosity has taken place, the strength and durability of the concrete significantly developed. In addition to Hutchison's [16] research in this area, and Sohn and Johnson [17] used MW energy to accelerate the curing process without incurring any significant loss of compressive strength in the cement mortar.

As a principal material in the production of concrete, water should be considered carefully in regard to the curing process. In particular, compared with the other components of concrete, water

has a relative dielectric constant ( $\epsilon'_r$ ) and loss tangent ( $\tan \delta$ ) with higher values. As a result, when the electric field  $\vec{E}$ , which is a main part of the electromagnetic field, interacts with the concrete's constituents, MW electromagnetic energy is quite dramatically transferred and then converted into heat via an interaction with water molecules. This mechanism causes the bonds of polar molecules to vibrate such that energy is dissipated as heat and transferred within the concrete workpiece to be processed, thus giving rise to accelerated hydration reactions. Consequently, free water molecules in the capillary pores of the concrete are quickly removed from the internal concrete structure before setting, which means that plastic shrinkage from drying is taking place. The result is the collapse of the capillary pores and microstructure simultaneously becomes more dense.

However, MW-assisted heating is still limited in terms of the types of concrete materials to which it can be applied. In this regard, Jeppson and Calif [18] reported that MW-assisted heating could only be used for conventional concrete. Until the present time, the non-uniformity of temperature distribution has been a main problem in attempts to use continuous MW heat in concrete applications [19]. The disadvantage of the dielectric materials is that its thermal distribution is inconsistent, which leads to problems associated with hot spots and cold zones [20]. Therefore, MW distribution with multi-mode cavity has been developed using MW technology applications whereby concrete is heated such that its moisture content evaporates while heat is transferred to its top surface.

The present research focuses on the design and construction of a portable prototype for concrete-accelerated curing that relies on applying MW energy. Experiments are performed, and the results are reported. The studied parameters are temperature evolution, moisture content, curing time, and compressive strength. Further, a comparison of MW curing and conventional (air or water) curing is also presented.

## 2. Design of a horn-shaped cavity using a mathematical model

It is generally accepted that uneven field distribution generates cold and hot spots and that the latter can contribute significantly to the phenomenon of runaway. For dielectric products (such as concrete), cold spots are unwelcome as they induce the internal structure to break or crack, thereby undermining the concrete's performance and rendering the concrete less durable. It is for this reason that a uniform electromagnetic heating is normally required. Researchers have devised multiple ways to improve the electric field as well as to improve heating distribution by varying the degree of achievement by changing either the source, the MW feeding system, the shape of the cavity, or the environment surrounding the load. Some ideas have been developed in regard to empty cavities; however, these do not work in applied situations [21]. For analysis, electromagnetic waves in the cavity were simulated to design the MW–vacuum system. The distributions of electric field strength and mode generation were studied in the simulation. The COMSOL MULTIPHYSICS® program version 3.4 [22] was used to construct domain meshes and the Finite Element Method (FEM) was employed to solve the problems. Generated resonant modes inside the multimode cavity, where the reflections from the cavity walls constructively reinforce each other to produce a standing wave, were calculated by determining the number of half-wavelengths in each of the principal directions. The quality factor (Q-factor) and the maximum electric field strength ( $E_{\max}$ ) were calculated by using the equations found in [19]. The time-average complex power flow through a defined closed surface was calculated from Poynting's theorem [23] when a MW source is connected to the cavity.

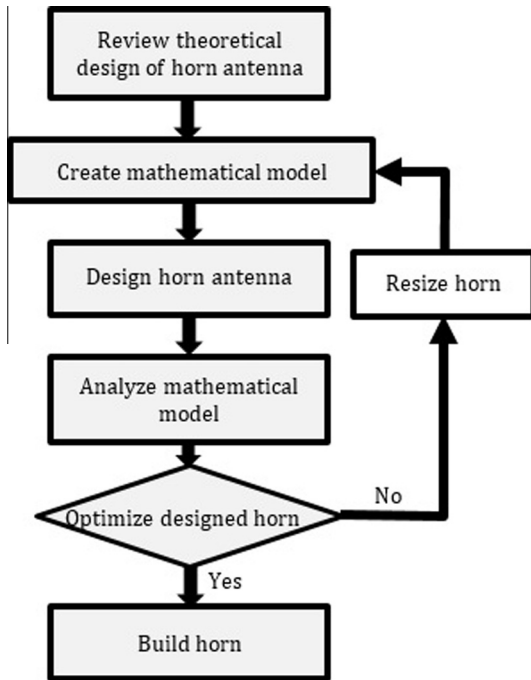


Fig. 1. Horn design process.

As shown in Fig. 1, in the present study, the design processes focus on the study of a horn-shaped cavity and a mathematical model to analyze and determine the horn size and configuration using the coupled electromagnetic and heat transfer analysis of both without load and with load (concrete workpiece) as shown below. A 3D mathematical model is considered, which is analyzed with COMSOL™ MULTIPHYSICS program version 3.4 [22]. After that, the MW-curing prototype is constructed. The horn of this prototype can be adjusted vertically. MW power of 800 W at 2.45 GHz is applied and fixed and movement modes are studied.

### 2.1. Mathematical formulation

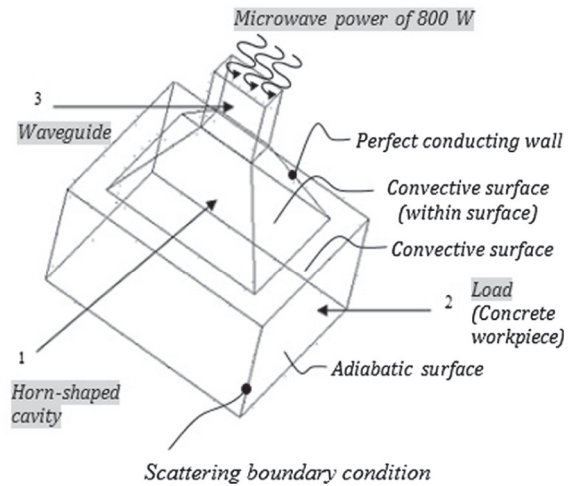
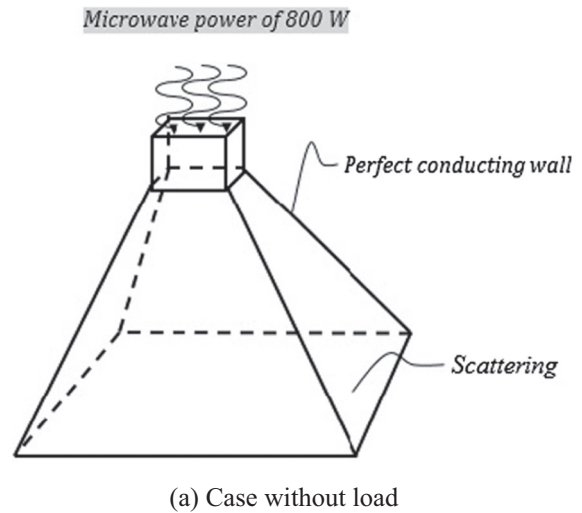
From the calculated horn size, the mathematical model is applied to determine the design size of the horn and to analyze the distribution of the electromagnetic field in the horn (without load case) and the distribution of the concrete's temperature (load case). In this study, COMSOL™ MULTIPHYSICS program version 3.4 [22] is used to create the mathematical model, beginning by calculating the horn size. Then, the mathematical model is used to analyze and determine the optimal horn size before the horn is built.

The mathematical model analysis is divided into two parts: a distribution analysis of the electromagnetic field in the horn and an analysis of the thermal distribution of the concrete. The physical domain is presented in Fig. 2 with the following input MW position:

- (a) The walls of the horn are perfect conductors.
- (b) The concrete (load) materials are non-magnetic.
- (c) The waveguide perfectly conducts the boundaries.

### 2.2. Analysis of the electromagnetic field in the horn

The distribution of the electromagnetic field in the horn (in terms of the waveguide, the horn, and the load) can be found by using Maxwell's electromagnetic field equation [24,25]. This can be carried out by using the COMSOL™ MULTIPHYSICS program version 3.4 [22], the equation associated with which is as follows:



(b) Case with load (concrete workpiece)

Fig. 2. Physical domain for analysis of the electromagnetic field in the horn and temperature distribution in the concrete. (a) Case without load. (b) Case with load (concrete workpiece).

$$\nabla \times (\mu_r^{-1} \nabla \times E) - k_0^2 \left( \epsilon_r - \frac{j\sigma}{\omega\epsilon_0} \right) E = 0 \quad (1)$$

$$\epsilon_0 = n^2 \quad (2)$$

where  $E$  is the electric field intensity (V/m),  $H$  is the magnetic field intensity (A/m),  $J$  is the current density (A/m<sup>2</sup>),  $\sigma$  is the electric conductivity (S/m),  $\mu_r$  is the relative magnetic permeability,  $\omega$  is the angular velocity (rad/s),  $k_0$  is the free space wave number,  $\epsilon_0$  is the permittivity of the vacuum ( $8.85419 \times 10^{-12}$  F/m),  $n$  is the refractive index, and  $\epsilon_r$  is the relative dielectric constant that expresses the properties of the material in terms of its absorption capacity to transmit and reflect MW energy.

#### 2.2.1. A case without load

The MW distribution in the waveguide and the horn constitutes the perfect conducting wall. Therefore, the electromagnetic boundary condition of the horn wall can be expressed as in this equation:

$$n \times E = 0 \quad (3)$$

The electromagnetic field condition created by the waveguide, an MW source, presented in Fig. 2, can be expressed as in this equation:

$$\text{port} : S = \int (E - E_1) \cdot E_1 / \int E_1 \cdot E_1 \quad (4)$$

where the port is the MW source at a power of 800 W.

The initial condition of the electromagnetic field is defined as:

$$E_x(t_0), E_y(t_0), E_z(t_0) = 0 \quad (5)$$

### 2.2.2. A case with load (concrete workpiece)

The coupled Maxwell's equation and heating model in this study is designed to analyze only the thermal distribution covering the concrete load under the electromagnetic field in the horn for the 3D case. On the assumption that the air in the horn cannot absorb the MW energy and transform it into heat, the internal load can transfer heat by conduction and the load can generate internal heat by transforming the MW energy into heat. On this assumption, the heat-exchange equation can be written based on the background from the COMSOL™ MULTIPHYSICS program version 3.4 [22] as in this equation:

$$\rho C_p \frac{\partial T}{\partial t} + \nabla \cdot (-k \nabla T) = Q \quad (6)$$

where  $T$  is the temperature (°C),  $t$  is time (s),  $C_p$  is the heat capacity at constant pressure (J/kg.K),  $\rho$  is the density (kg/m<sup>3</sup>),  $k$  is the thermal conductivity (W/m.K), and  $Q$  is the local volumetric heat-generation term generated by the absorption of the MW energy transmitted as heat (W/M<sup>3</sup>).

The outer sides of the calculated domain, i.e., the free space, are considered to be the scattering boundary condition as expressed in this equation:

$$\begin{aligned} n \times (\nabla \times E) - jkn \times (E \times n) = \\ -n(E_0 \times Jk(n - k))(\exp(-Jk \cdot r)) \end{aligned} \quad (7)$$

Heat can only be generated by the load or the concrete; therefore, the considered domain in terms of heat focuses directly on load. Thus, the boundary condition of heat occurs only on the top surface of the load (the wall of the load is an insulator, which cannot transmit heat).

The boundary condition of the heat surface at the top of the load (concrete workpiece) is

$$n \cdot (-k \nabla T) = 0 \quad (8)$$

The boundary condition of the heat wall is

$$-n \cdot (-k \nabla T) = 0 \quad (9)$$

The initial condition of the heat analysis is

$$T(t_0) = 303.15 \text{ K} \quad (10)$$

## 3. Materials and methods

Concrete was mixed and poured into molds. Two kinds of cases were explored: conventional curing (air curing and water curing) and MW curing (fixed and movement modes).

### 3.1. Materials

All the materials used in this study were obtained locally. The cementitious material used in all the mixtures was Type 1 Portland cement (OPC), which complies with ASTM C 150 [26]. The chemical compositions and physical properties of the cement are listed in Table 1. The tap water used conforms to ASTM C 1602 [27]. Further, the fine and coarse aggregates also obtained locally as river sand and crushed limestone rock, respectively, were in accordance with ASTM C 33 [28]. A mix proportion per one cubic meter of concrete used is shown in Table 2.

**Table 1**  
Chemical composition and physical properties of Type 1 Portland cement.

Chemical composition (% by mass)	Type 1 Portland Cement (OPC)
Silicon dioxide (SiO <sub>2</sub> )	16.39
Alumina oxide (Al <sub>2</sub> O <sub>3</sub> )	3.85
Ferric oxide (Fe <sub>2</sub> O <sub>3</sub> )	3.48
Magnesium oxide (MgO)	0.64
Calcium oxide (CaO)	68.48
Sodium oxide (Na <sub>2</sub> O)	0.06
Potassium oxide (K <sub>2</sub> O)	0.52
Sodium oxide (SO <sub>3</sub> )	4.00
Titanium dioxide (TiO <sub>2</sub> )	N/D*
Physical properties	
Loss on Ignition (% by mass)	1.70
Particle size distribution (D [4,3] μm)	23.32
Bulk density (kg/m <sup>3</sup> )	1550
Specific gravity	3.20
Specific surface area (m <sup>2</sup> /kg)	610

\* N/D indicates "Not Detected".

**Table 2**  
Mixture proportion of concrete (per 1 cubic meter of concrete).

Portland Cement (kg)	Water (kg)	River sand (kg)	Crushed limestone rock (kg)	Water-cement ratio (by mass)
350	170	830	1135	0.486

### 3.2. Equipment

The mobile MW-curing unit for concrete curing is constructed based on coupled MW-thermal analysis in Eqs. (1)–(10) both the without load and with load as presented in Fig. 3. The applied frequency of the MW is 2.45 GHz, which is created by a horn with a magnetron waveguide installed. The power is set at 800 W to produce MW energy. A programmable logic controller (PLC) system is applied to control the movement and on-off mode. The length of the rail is 2.5 m, and a motor to control the driving, AC type, 90 W is installed. A chain is used for driving and use gear (13 pieces that have a gear ratio of 1:5), and the motor drive speed is 5 round/min (rpm.)

### 3.3. Concrete workpiece preparation

The mixture is weighed, mixed, and poured into an acrylic mold with a thickness of 10 mm, which is designed to protect the mixture from the reflection of the MW. The dimensions of the mold are 150 × 150 × 150 mm, as stated in the British standard BS 1881: Part 3 [29]. The concrete is mixed according to the ASTM C 192 standard [30]. The mixture is left to develop for an initial setting time of 30 min, after which it is cured using MW energy. Next, the frame is removed from the mold, and the curing continues but now in the air by wrapping the mixture in a sealed plastic bag and keeping it at a temperature of 25 ± 2.0 °C for 12 h. Finally, the compressive strength of the mixture is tested.

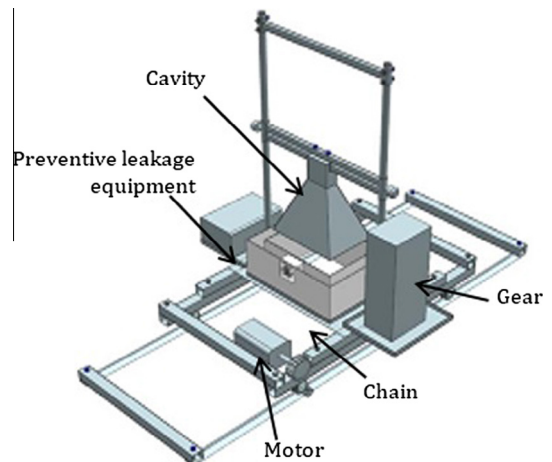


**Fig. 3.** Prototype for moving mode MW curing.

**Table 3**  
Cases and conditions for concrete curing.

Case	Power (W)	Preheating (minutes)	Pause (minutes)	Heating (minutes)	Total (minutes)
Case A	Air, Water	–	–	–	8 h, and 1, 3, 7, 14, 28 days
Case B	800	Continuity	–	–	30, 60, 90, 120
Case C	400	Continuity	–	–	30, 60, 90, 120
Case D	800	20	120	10	30, 60, 90, 120
Case E	800	30	60	15	30, 60, 90, 120
Case F	800	30	60	10	30, 60, 90, 120

Similarly for curing in water and air, the mixture is poured into a steel mold and cured for  $23\frac{1}{2} \pm \frac{1}{2}$  h. Then, some concrete workpieces of the mixture are cured in water for respective periods of 8 h, 1 day, 3 days, 7 days, 14 days, and 28 days. Other concrete workpieces are cured in air such that they are wrapped and sealed in a plastic bag and kept in a controlled room where the temperature is maintained in the range of  $25 \pm 2.0$  °C and relative moisture is maintained in the range of  $60\% \pm 5.0\%$ . These workpieces are cured for respective periods of 8 h, 1 day, 3 days, 7 days, 14 days, and 28 days. Finally, the compressive strength of the concrete is tested.

### 3.4. Cases used to study MW curing

In this study, concrete curing is tested via a conventional method and via MW curing in both the fixed and movement modes. Non-continuous MW curing is carried out in the preheating phase by using MW energy for a fixed period. Then, the heating is paused and the concrete is reheated using MW power. The conditions in which the curing took place are presented in Table 3. The details of each experiment are as follows:

- *Case A: Concrete curing in water and air*

For concrete curing in water and air, the frame is removed from the mold when the mixture is at age  $23\frac{1}{2} \pm \frac{1}{2}$  h. For water curing, the testing times are 8 h, 1 day, 3 days, 7 days, and 28 days. For air curing, the concrete is wrapped and sealed in a plastic bag and kept in a controlled room where the temperature is held at  $25 \pm 2.0$  °C and where the relative moisture is held at approximately  $60\% \pm 5.0\%$ . The curing is carried out for 8 h, 1 day, 3 days, 7 days, 14 days, and 28 days. Finally, the compressive strength of the concrete is tested.

- *Case B: Concrete curing by using continuous MW power of 800 W*

The concrete is cured by using continuous MW power of 800 W and tested at 30, 60, 90, and 120 min.

- *Case C: Concrete curing by using continuous MW power of 400 W*

The concrete is cured by using continuous MW power of 400 W and tested at 30, 60, 90, and 120 min.

- *Case D: Concrete curing by using non-continuous MW power of 800 W*

The concrete is cured by using non-continuous MW power of 800 W and tested at 30, 60, 90, and 120 min (not including the pause time). The PLC system is used to control the on-off switch for the MW power.

- *Case E: Concrete curing by using non-continuous MW power of 800 W*

The concrete is cured by using non-continuous MW power of 800 W and tested at 30, 60, 90, and 120 min (not including the pause time). The PLC system is used to control the on-off switch for the MW power.

- *Case F: Concrete curing by using continuous MW power of 800 W (movement system)*

The concrete is cured by using MW power of 800 W, and the PLC system is used to control the on-off switch for the MW power and the movement, as shown in Fig. 4. There are six workpieces, each of which is cured by MW energy for 180 min.

### 3.5. Testing methods

#### 3.5.1. Moisture content measurement

The moisture content is measured is based on the weight of the mixed cubic concrete to find the initial weight of the concrete workpiece. After that, each workpiece is wrapped and sealed in a plastic bag and kept at a temperature in the range

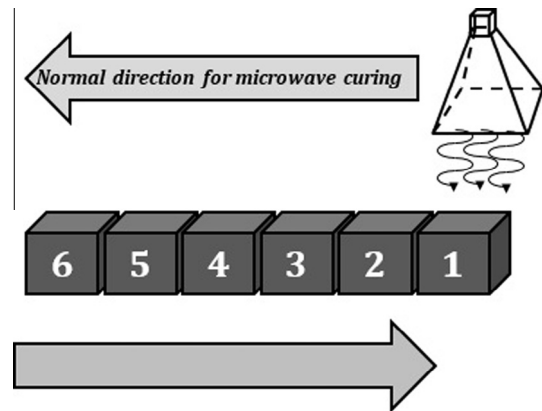


**Fig. 4.** Flow diagram of process for MW-curing of concrete (movement steps).

of  $25 \pm 2.0$  °C for 12 h. Then, the concrete is weighed to determine the final weight, after which the compressive strength is tested. Further, the wet bulb in the concrete can be calculated by using the following equation:

$$A = \left( \frac{W_a - W_b}{W_a} \right) \times 100 \quad (11)$$

where  $A$  is the wet bulb (%),  $W_a$  is the initial weight of the concrete before curing (kg), and  $W_b$  is the final weight after curing (kg).

#### 3.5.2. Temperature measurement

The temperature measurement of the concrete can be divided into two aspects: the internal temperature measurement and the external temperature measurement. The process of measuring begins by using a system for measuring temperature connected to a data logger and spike in the middle of the concrete. Three levels of concrete, the top, middle, and bottom, are all measured at 30, 60, 90, and 120 min.

The measurement is carried out at 1 cm from the top surface (top), 7.5 cm from the top surface (middle), and 14 cm from the top surface (bottom), as presented in Fig. 5. The natural heat advection is assumed at the top surface because the wall side is insulated by the 10 mm thick acrylic. In addition, heat transpiration occurs only at the top surface and not at the sides. The internal temperature is measured in order to establish the effect of the MW-curing temperature for Cases B, C, D, and F.

#### 3.5.3. Compressive strength test

Compressive strength—the maximum stress concrete can bear before cracking—is the most important property of concrete. The respective processes for testing the compressive strength of concrete by air curing, water curing, by MW curing are carried out by following the standard set out in BS 1881[31].

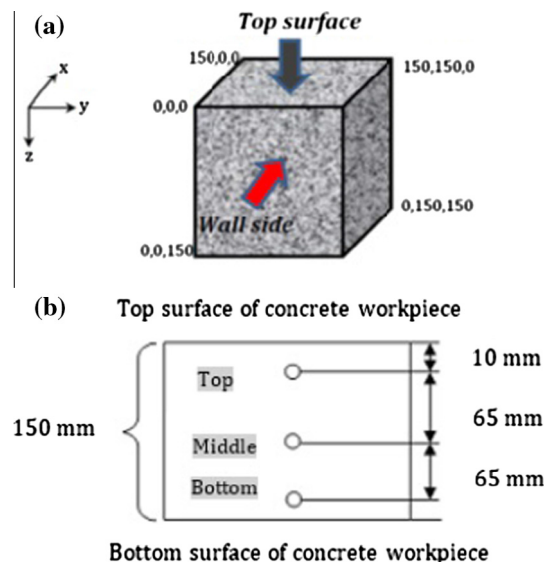


**Fig. 5.** (a) Dimension of specimen (mm). (b) Installation of a measuring temperature system for measuring the internal temperature of concrete.

### 4. Model simulation of horn

#### 4.1. Analysis of the horn size

The analysis of the horn size is divided into two parts: an analysis of the distribution of the electromagnetic field within the horn (without load) and an analysis of the thermal distribution of the concrete (with load). Time does not affect the electromagnetic field behavior covering the concrete workpiece in this analysis, but time does affect the distribution of the electromagnetic field covering the concrete workpiece. Thus, this is a steady-state problem. Therefore, the analysis of the distribution of the electromagnetic field covering the concrete workpiece in 3D is carried out using the COMSOL™ MULTIPHYSICS program version 3.4 [22].

In the analysis of the thermal distribution in the concrete, it was found that time had a direct effect on the temperature of the load. This problem is identified as a transient condition. Therefore, the analysis of the distribution of the concrete temperature is performed with the finite element method using the COMSOL™ MULTIPHYSICS program version 3.4 [22].

The input data used to analyze both the electromagnetic field and the heat transfer are presented in Table 4.

#### 4.2. Calculation procedure

In this study, the finite element method is used to analyze the transient problems. The computational scheme is to assemble a

**Table 4**  
Input data for analysis.

Symbol	Value	Unit	Ref.
$\epsilon_0$	$8.85419 \times 10^{-12}$	F/m	–
$\mu_0$	$4\pi \times 10^{-7}$	H/m	–
$\epsilon_r$	10	–	[Measured by Authors]
$t$	60	s	–
$c_p$	650	J/kg.K	[Measured by Authors]
$\rho$	2300	kg/m <sup>3</sup>	[Measured by Authors]
Power	800	W	–
$f$	2.45	GHz	–
$T(t_0)$	303.15	K	–
$k$	0.87	w/m.K	–

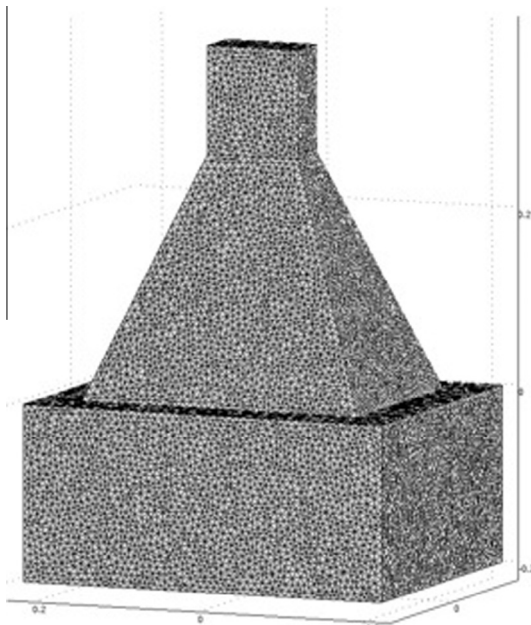


**Fig. 6.** A three-dimensional finite element mesh of horn and concrete model.

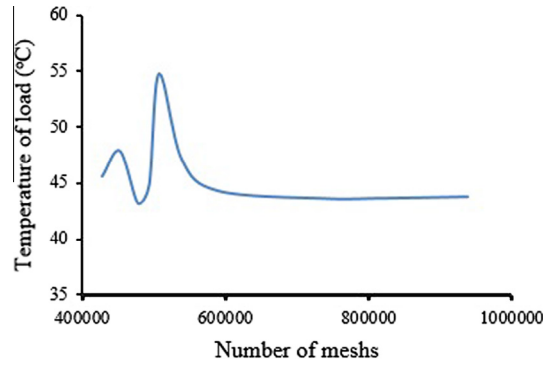


**Fig. 7.** Grid convergence curve of the 3D model.

finite element model and compute a local heat generation term by performing an electromagnetic calculation using concrete properties.

In order to obtain a good approximation, a fine mesh is specified in the sensitive areas. This study provides a variable mesh method for solving the problem as shown in Fig. 6. The model of heat equation and Maxwell’s equation is then solved. All computational processes are implemented using COMSOL™ MULTIPHYSICS program version 3.4. The electromagnetic power absorption at each point is computed and used to solve the time-dependent temperature distribution. All steps are repeated, until the required exposure time is reached. Convergence tests of the frequency of 2.45 GHz case are carried out to identify a suitable number of elements required. The convergence curve resulting from the convergence test is shown in Fig. 7. This convergence test leads to a grid with approximately 700,000 elements. It is reasonable to assume that, with this element number, the accuracy of the simulation results is independent of the number of elements.

### 5. Results and discussion

In this section, the modeling results of the electromagnetic field and the results of the tests focused on the thermal behavior of concrete during MW curing.

#### 5.1. Results of the model simulation

The modeling results of the electromagnetic field within the horn in the shape of a horn (without load case) (Fig. 8(a) and the thermal distribution covering the concrete workpiece (with load case) are presented in Fig. 8(b).

In Case 1 (Adjustment on the height of horn), the electric fields are  $8.006e^4 \times 10^4$  V/m,  $1.062e^5 \times 10^5$  V/m,  $1.128e^5 \times 10^5$  V/m, and  $8.729e^4 \times 10^4$  V/m, as presented in Fig. 4. The electric fields are similar whereas the increased distribution of the electric field by an increase in the height of the horn from 211.8 to 273 mm provides a progressive electric distribution of  $8.729e^4 \times 10^4$  V/m, as presented in Fig. 9(d).

In regard to the thermal distribution in the concrete, it was found that the increased horn height in Fig. 10 produced a temperature of  $\lambda/4$ ,  $\lambda/2$ ,  $3\lambda/4$ ,  $\lambda$  at 64.782, 63.809, 71.743, and 67.481 °C, respectively. When the horn height is increased by  $\lambda$  to achieve a height of 273 mm, as presented in Fig. 10(d), the thermal distribution in the surface of the concrete improves, i.e., becomes more even. In addition, the thermal distribution widens and hot and cold spots are reduced, as presented in Fig. 10.

It is emphasized that the height adjustment of the horn produces an electric field of  $8.729e^4 \times 10^4$  V/m, as presented in Fig. 9 (d), and a thermal distribution at 67.481 °C. After this height optimization, the horn width is adjusted by taking the steps described next.

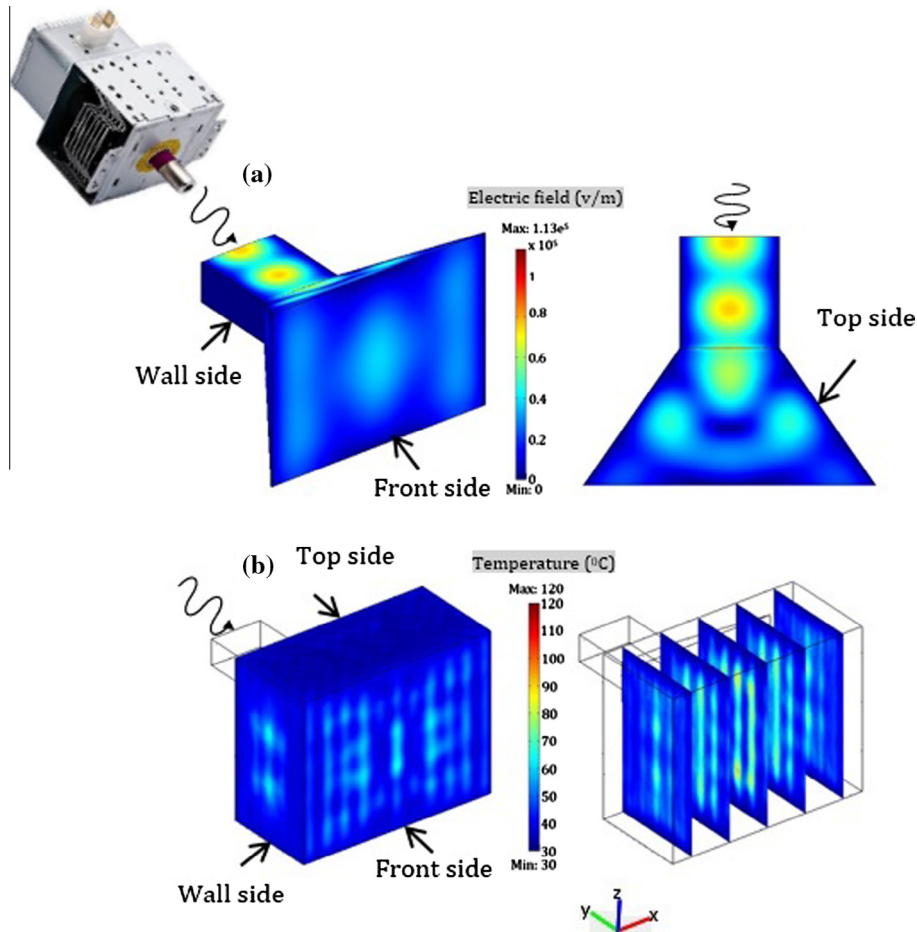


**Fig. 8.** (a) Distribution of electromagnetic field at a MW power of 800 W within the horn (without load) from the first result of the horn design. (b) Temperature distribution (with load) integrated with the first horn design.

For the simulation in Case 2 (decreasing adjustment on the width of horn), the electric fields are  $8.892 \times 10^4$  V/m and  $9.05 \times 10^4$  V/m when the horn width is increased, as presented in Figs. 11(a) and 6(b), respectively. In Fig. 11(a), it is shown that the increased horn width produces uniform electric distribution in terms of the electric field. In addition, the distribution of the concrete temperature found at  $73.092^\circ\text{C}$  is presented in Fig. 11 (c) and that found at  $69.076^\circ\text{C}$ , in Fig. 11(d). Therefore, if the horn width is increased, as presented in Fig. 11(a), the electric field in the horn will increase. This increase, in turn, facilitates the process whereby the material or load can receive the electric field, which can produce the concrete thermal distribution and increase the thermal distribution at the surface.

For Case 3 (increasing adjustment on the width of horn), the electric fields of the reduced-width horn, as presented in Fig. 12 (a) and (b), are  $8.387 \times 10^4$  V/m and  $9.579 \times 10^4$  V/m, respectively. It was found that if the horn width is reduced, the size of the electric field decreases. The thermal distribution covering the concrete load is  $73.307^\circ\text{C}$  and  $81.764^\circ\text{C}$ , as presented in Fig. 12 (c) and (d), respectively.

With the horn design based on the concept of an antenna, the electric distribution within the horn is  $7.625 \times 10^4$  V/m, as presented in Fig. 8(a), and the temperature of the load/concrete is  $63.731^\circ\text{C}$ . After increasing the horn height, increasing and reduction of horn found that the electric field is  $8.892 \times 10^4$  V/m, as presented in Fig. 11(a), and the concrete temperature is  $73.092^\circ\text{C}$  showing increasing the distribution of electricity, or multimode wave and temperature. The temperature at the center of the concrete for first horn design and adjusted horn of  $246.7 \text{ mm} \times 333.68$

mm, as presented in Figs. 13 and 14, respectively. It was found temperatures along the x, y and z axis of horn ( $246.7 \text{ mm} \times 333.68 \text{ mm}$ ) consistently over.

## 5.2. Results of the experiments

The results of the thermal behavior of concrete during MW curing, the thermal distribution on the concrete surface, the residual moisture content after MW curing, and the compressive strength of the concrete are discussed.

### 5.2.1. Thermal behavior of concrete under MW curing (Case B)

Fig. 15 presents the effects of MW curing of concrete with a 0.48 water–cement ratio under a 120 min curing time and 800 W (Case B). It is found that the temperature of the concrete increased continuously. At the beginning of the experiment, the moisture content of the concrete is high, which means that the transfer rate of MW energy to heat takes place rapidly in accord with heat production theory [19]. After 90 min, the temperature is constant because the moisture content at the surface of the concrete is reduced due to the absorption capacity of the MW energy. It can be explained that the dielectric property of concrete is related to the reduced moisture whereas the internal structure of the concrete's voids means that excess water is retained (i.e., the free or residual water remaining after the chemical reaction). After being activated by the MW energy, the concrete is absorbed and transmits heat energy. At the beginning of the curing process, the moisture content in the concrete has a direct effect on the initial temperature because the concrete's dielectric property is high. This causes the concrete's

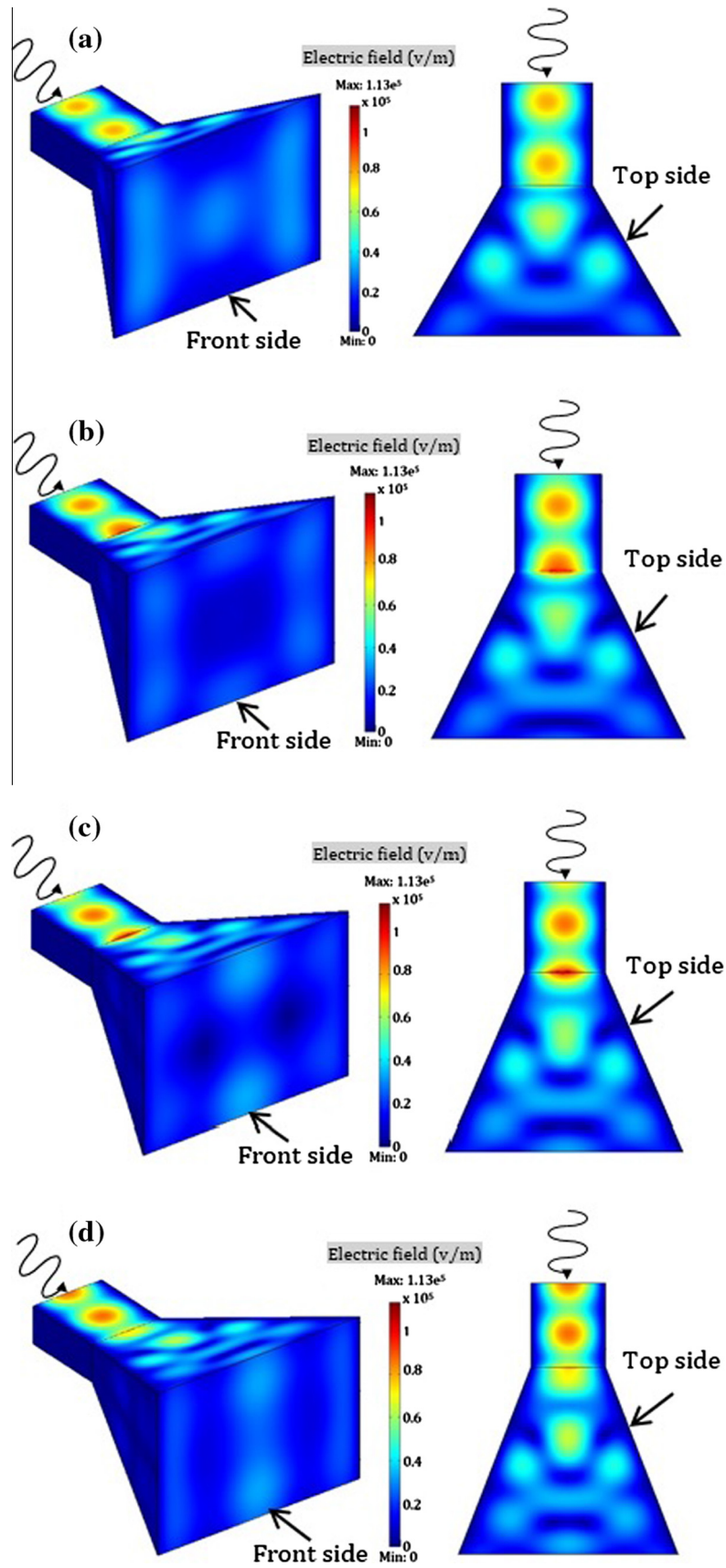


**Fig. 9.** Distribution of electromagnetic field at a MW power of 800 W within the horn (without load) of (a) Height of original horn of  $\lambda/4$  is equal to 181.2 mm. (b) Height of original horn of  $\lambda/2$  is equal to 211.8 mm. (c) Height of original horn of  $3\lambda/4$  is equal to 242.4 mm. (d) Height of original horn of  $\lambda$  is equal to 273 mm.

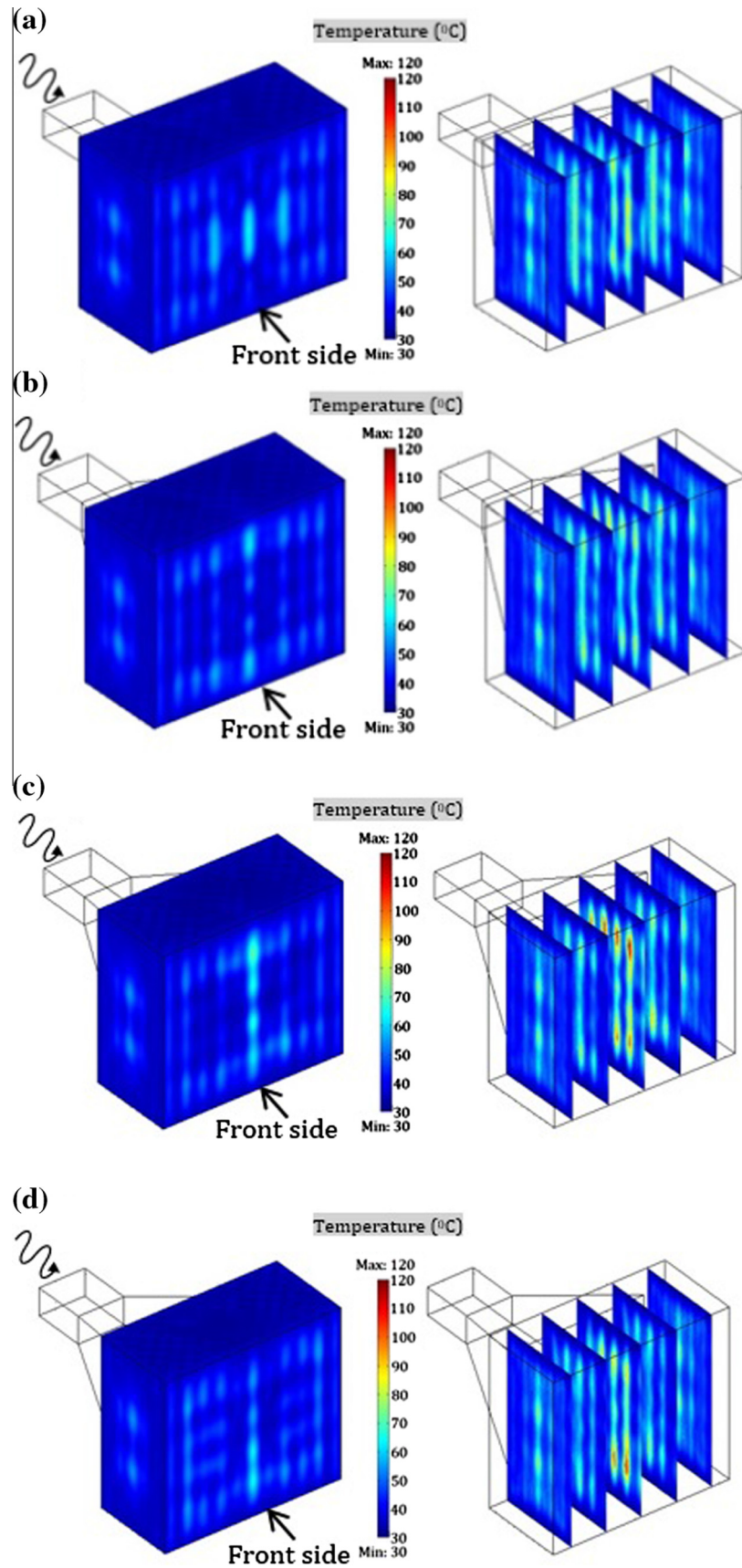


**Fig. 10.** Temperature distributions at a MW power of 800 W within the horn at (a) height  $\lambda/4$  is equal to 181.2 mm (b) height  $\lambda/2$  is equal to 211.8 mm. (c) height  $3\lambda/4$  is equal to 242.4 mm. (d) height  $\lambda$  is equal to 273 mm.

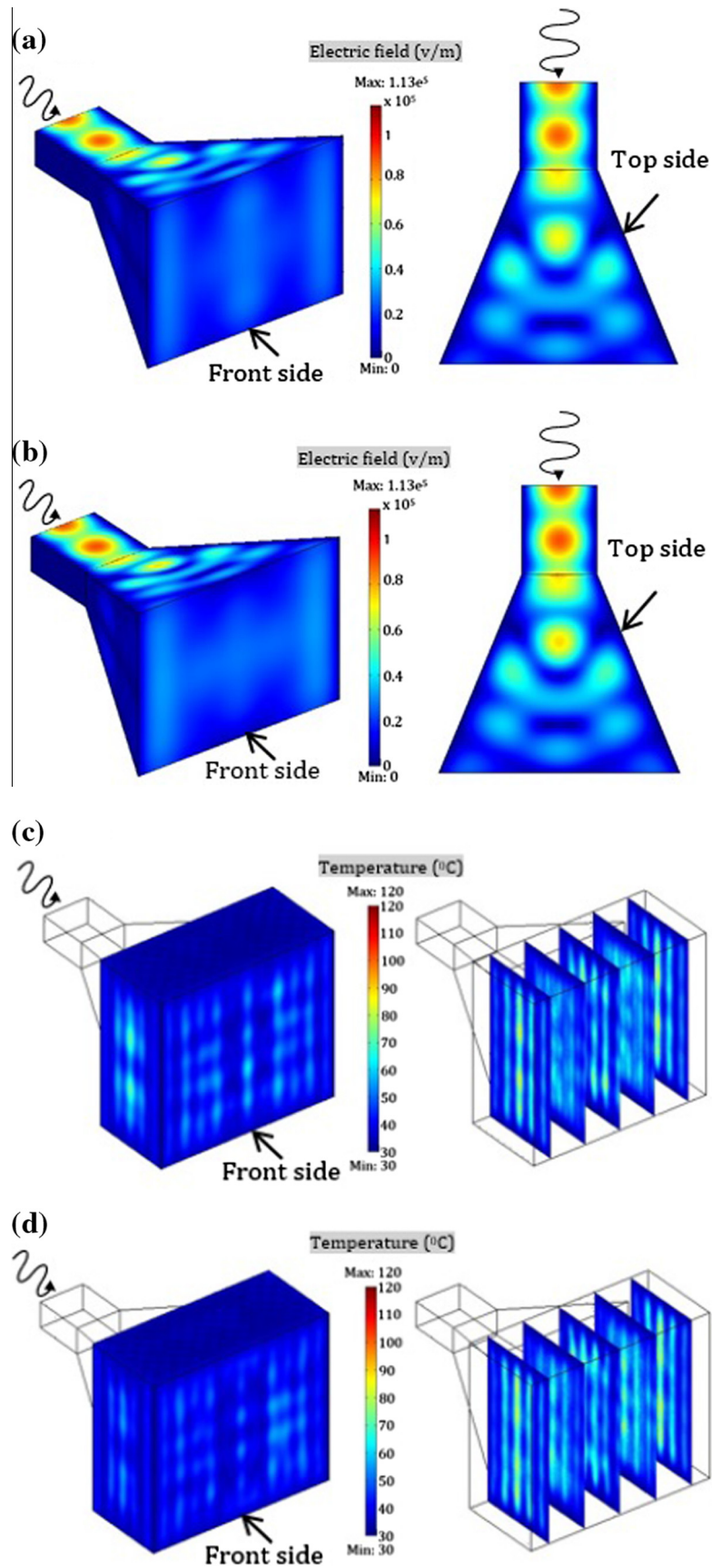


**Fig. 11.** Distribution of electromagnetic field of (a) adjusted horn of 246.7 mm × 333.68 mm, (b) adjusted horn of 256.7 mm × 347.2 mm, and temperature distributions of (c) adjusted horn of 246.7 mm × 333.68 mm and (d) adjusted horn of 256.7 mm × 347.2 mm.

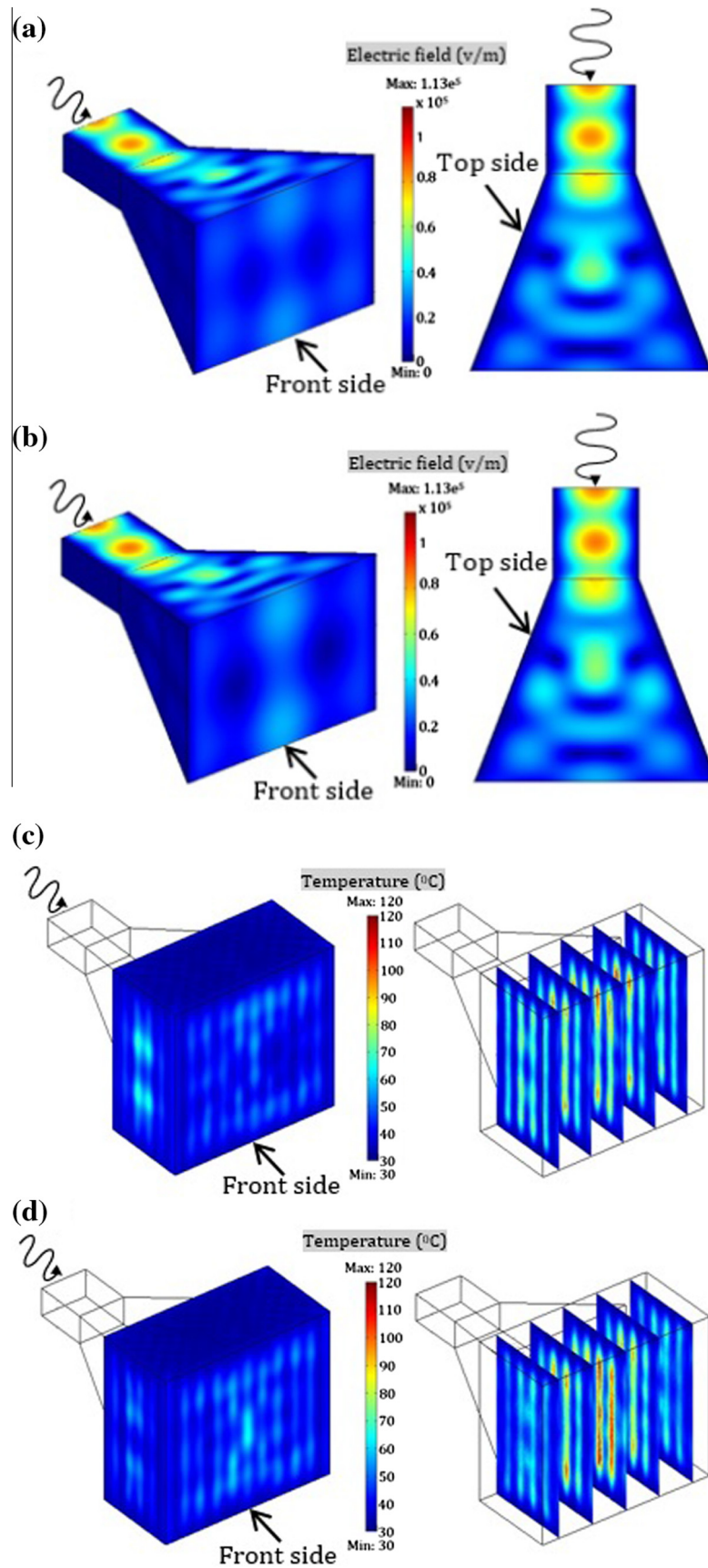


**Fig. 12.** Distribution of electromagnetic field of (a) Reduction of horn size of 226.7 mm × 306.64 mm, (b) Reduction of horn size of 216.7 mm × 293.12 mm, and temperature distributions of (c) Adjustment of horn size of 226.7 mm × 306.64 mm and (d) Reduction of horn size of 216.7 mm × 293.12 mm.

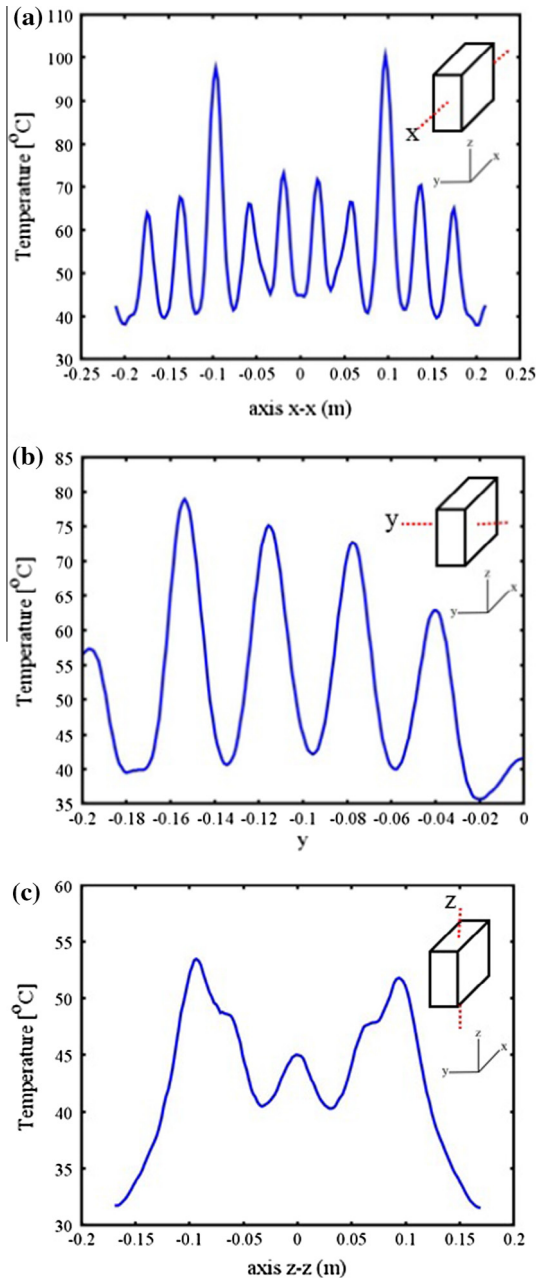


**Fig. 13.** Temperature at the center of the concrete for first horn design. (a) Temperatures along the x axis. (b) Temperatures along the y axis. (c) Temperatures along the z axis.

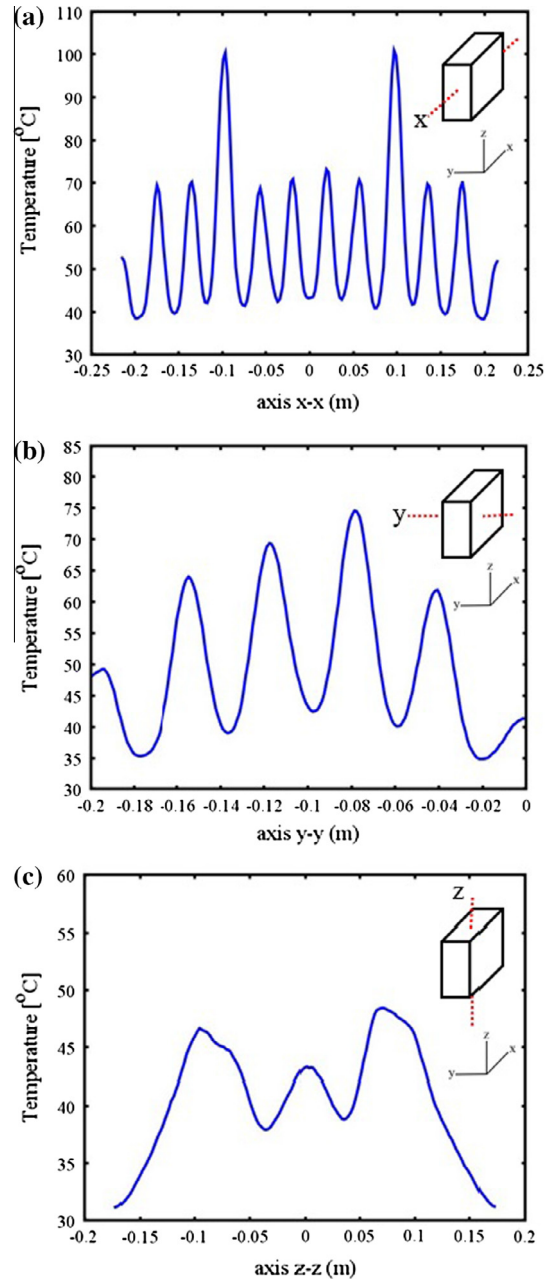


**Fig. 14.** Temperature at the center of the concrete for adjusted horn of 246.7 mm × 333.68 mm. (a) Temperatures along the x axis. (b) Temperatures along the y axis. (c) Temperatures along the z axis.

temperature to increase rapidly and continuously. However, as the moisture content in the concrete decreases, the dielectric property also decreases, rendering the concrete's temperature constant.

At the beginning of the curing process, the temperature at the top of the concrete increases continuously whereas the temperature in the middle increases intermittently. It can be explained that the top surface contains excess water and that bleeding occurs after curing for 30 min to develop initial setting time. At this stage, the concrete surface absorbs the MW energy to a significant extent after 70 min of curing. However, the temperature in the middle increases rapidly because the temperature of 100 °C at the top surface is high enough to transfer as far down as the middle. In addition, heat accumulates in the middle of the concrete and heat cannot occur because of the insulation wall. At the bottom, the temperature increases slowly due to the heat accumulation and the insulation wall. However, at 95 min, the heat increases dramati-

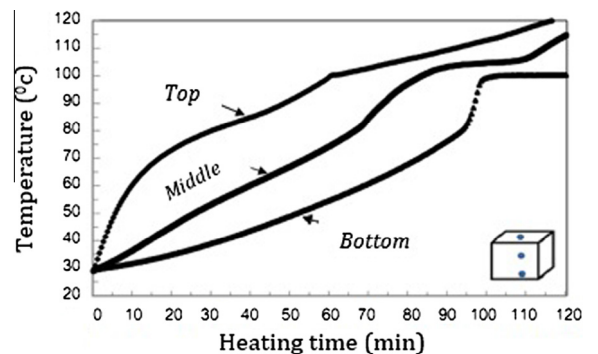


**Fig. 15.** Temperature profile of concrete during continuous MW curing with clapsed time and 800 W (Case B).

ically from 70 °C to 100 °C. The temperature at the top surface is 110 °C, and in the middle it is 103 °C. Therefore, the heat transfer is conducted throughout the concrete workpiece. Then, at 100 min, the temperature throughout the concrete increases to 100 °C. In addition, at 120 min, the temperature at the top surface is 125 °C, in the middle it is 110 °C, and at the bottom it is 100 °C.

### 5.2.2. Influence of MW power on the temperature of concrete under MW curing (Case C)

Fig. 16 presents the results from the MW curing of concrete at 400 W. The results show that the temperature of the concrete increased rapidly due to a change in the amount of electrical power used directly reduces the multi-mode within the horn. Curing the concrete for 30 min at 400 W can increase the concrete's temperature to 70 °C, whereas curing by 800 W for 30 min can increase the concrete's temperature to 80 °C. It was found that the behavior of heat generation within the concrete under both of these conditions is quite similar. At the beginning of the process, the temperature at the top surface is very high due to the high moisture content and the high dielectric property of the concrete, which MW energy can absorb and transform entirely into heat energy. The temperature in the middle of the concrete increases continuously due to penetrated MW can increase the concrete temperature. Heat accumulates at the bottom of the concrete because of the insulation wall and the heat transferred from the surface. After 70 min, the temperature in the middle changes rapidly due to a top surface temperature of 105 °C. Then, the difference in temperature in the middle and at the bottom is constant because 400 W is used to absorb the MW energy of the dielectric material, which is directly related to the electric field. Therefore, heat generation in the concrete decreases. At the bottom, the temperature is constant at 100 °C after 90 min, indicating that electrical or MW power influences the heat generation of concrete due to changes in the electric field.

### 5.2.3. Thermal behavior of concrete under discontinuous concrete curing (Case D)

In this experiment, the concrete is tested in both the fixed mode and the movement mode at 800 W (Case B). The results show that the concrete's compressive strength decreases continuously after a curing time of 90 min and again after 120 min. When the concrete's temperature is higher than 80 °C [17], compressive strength decreases by 50%. By observation, at a curing time of 120 min, it was found that the temperature at the top, middle, and bottom of the concrete was 125, 115, and 100 °C, respectively. These results may have a negative effect on the internal structure of the concrete, which may crack thereby giving rise to low compressive strength. Therefore, discontinuous MW curing is applied in order to maintain the appropriate temperature, which can increase the compressive strength of concrete. This experiment was carried

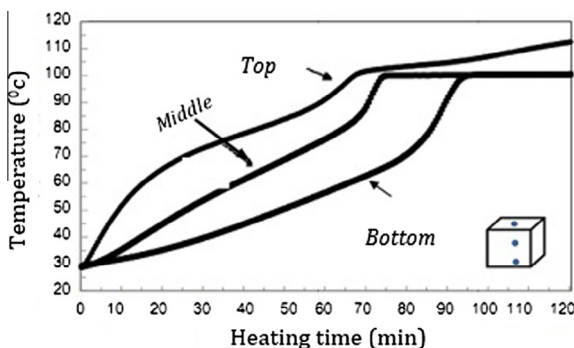


Fig. 16. Internal temperature of concrete during continuous curing by MW energy with clapsed time and 400 W (Case C).

out by using the PLC system to control the MW supply or on-off mode, as presented in Fig. 17.

Fig. 17 presents the discontinuous curing by MW energy case (Case D). The experiment is carried out by preheating the workpieces for 20 min, followed by idle time for 2 h, and then energizing by MW power for 10 min and idle time for 2 h until the total time is 2 h. The total time of this experiment is 22 h, and the total MW curing time is 120 min. The results show that in the first 20 min, the temperature at the top, in the middle, and at the bottom of the concrete is approximately 68, 50, and 43 °C, respectively. After that, the PLC serves the function of stopping the MW supply for 2 h and of reheating the workpieces for 10 min. This working loop is operated for 120 min (including only the energizing time and excluding the idle time). During the idle time, the temperature at the top, in the middle, and at the bottom decreases to 20, 10, and 5 °C, respectively. These phenomena can be explained by noting that the top surface is exposed to air because of heat advection, such that the temperature decreases. The temperature in the middle decreases slowly and at the bottom the temperature decreases slightly as there is no heat advection.

### 5.2.4. Heat evolution from discontinuous curing (Case E)

Fig. 18 presents the discontinuous curing by MW energy case (Case E). In this experiment, the moisture content still retained in and the compressive strength of the concrete increased slightly. Therefore, the energizing time of MW is added and idle time is reduced in order to achieve a high temperature and remove moisture. The experiment is carried out by MW energizing for 30 min, idle time for 1 h, and re-energizing for 15 min followed by a second idle time of 1 h until the total time reaches 120 min. The total time

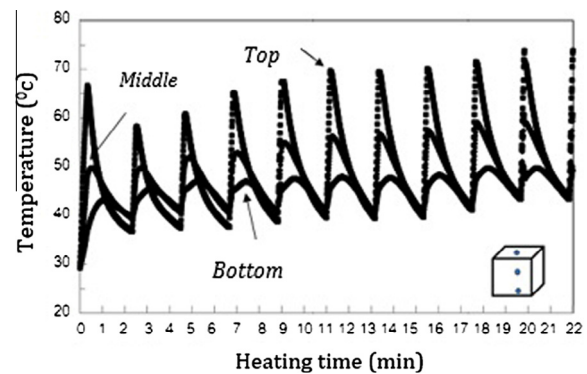


Fig. 17. Temperature of concrete during discontinuous curing by preheating for 20 min, idle time for 2 h, energized by MW power for 10 min and idle time for 2 h (total time of this experiment is 22 h, and the total MW curing time is 120 min).

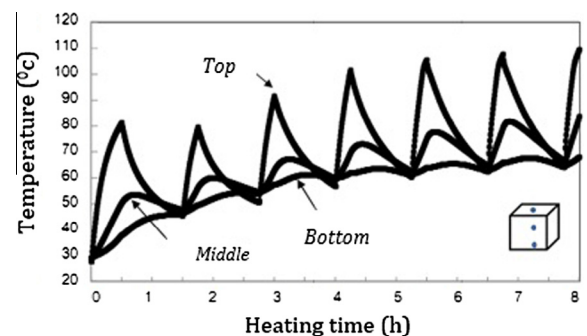


Fig. 18. Internal temperature of concrete after discontinuous MW curing (Case E) by MW energizing for 30 min, idle time for 1 h and re-energizing for 15 min and second idle time for 1 h until the total time reaches 120 min. Total time is 8 h, and curing time is 120 min.

is 8 h, and the curing time is 120 min, which is controlled by the on-off system of the PLC. In the first 30 min, the temperature at the top, in the middle, and at the bottom is 81, 55, and 41 °C, respectively. The operating loop consists of 1 h of idle time and 15 min of energizing MW. The results show that temperature increased continuously because the energizing time was increased and the idle time was reduced. The temperature at the top, in the middle, and at the bottom was 110, 83, and 65 °C, respectively. In addition, the moisture content and the compressive strength of the concrete were both higher than these respective properties under discontinuous curing (Case D).

5.2.5. Thermal distribution at the concrete surface

The internal temperature of the concrete after MW curing is carried out by measuring the temperature in various parts of the workpieces. The absorption phenomenon where by MW energy is transformed into heat energy while the temperature increases continuously is shown in Fig. 19 (Case B). There was two hot spot zone in time 60 min in Fig. 19(b) and one hot spot zone in Fig. 19(c).

The external temperature at the top surfaces and sides of the workpieces is recorded by using an infrared camera. The results indicate that heat in the concrete wall is evident at a depth of 3

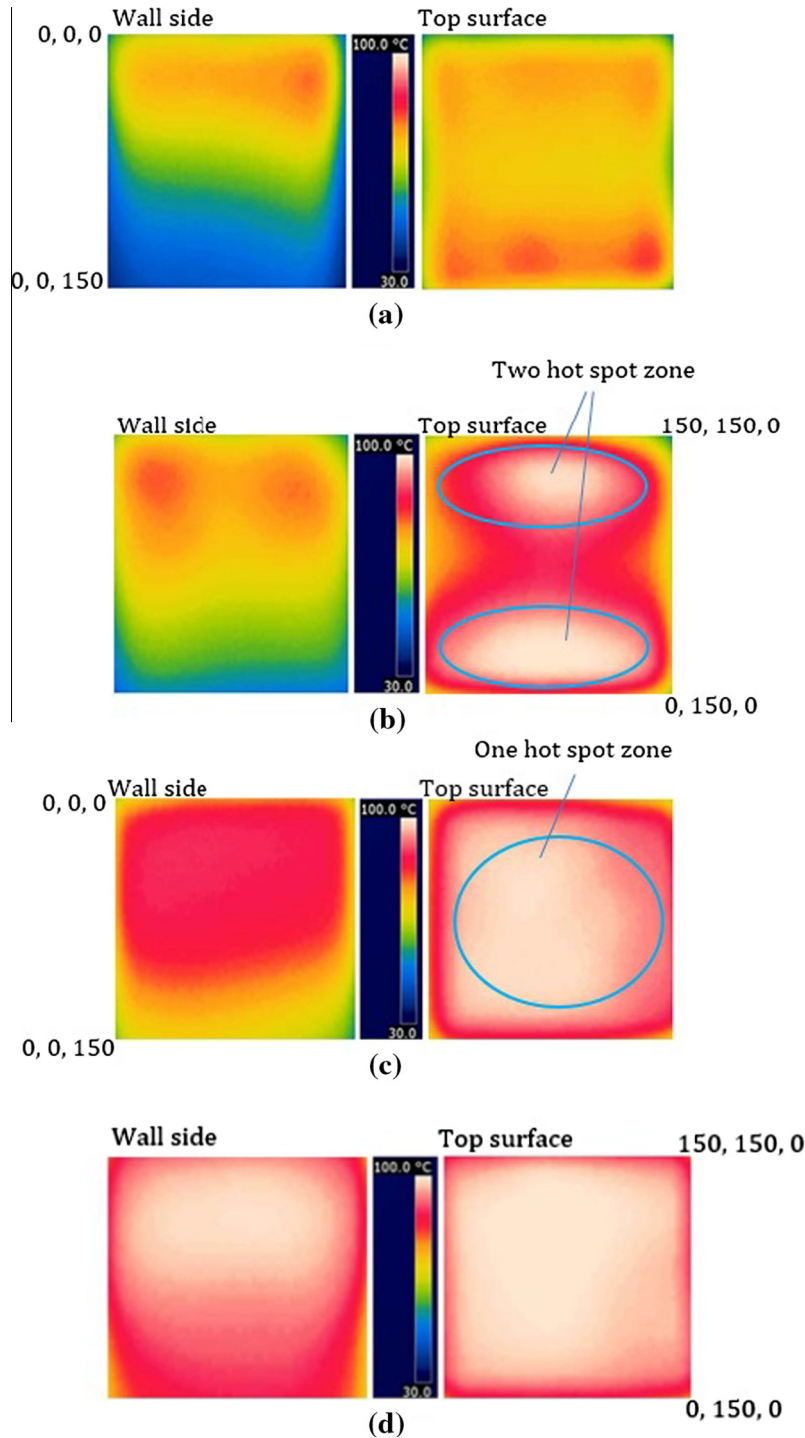
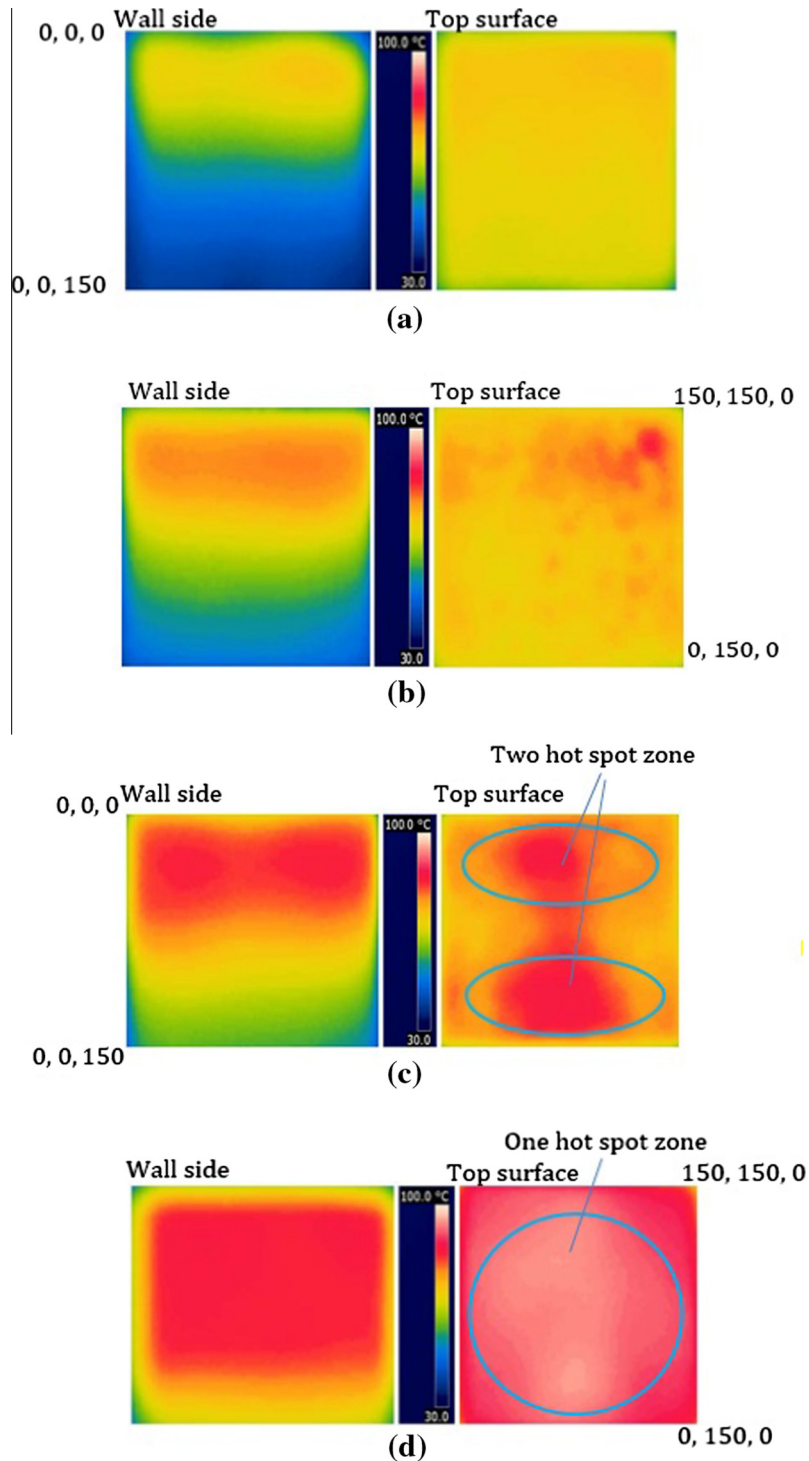


Fig. 19. Temperature distribution at the top surface and wall side after continuous MW curing at 800 W of Case B for (a) 30 min, (b) 60 min, form two hot spot zone. (c) 90 min, form one hot spot zone and (d) 120 min.



**Fig. 20.** Temperature distribution after continuous MW curing at 400 W of Case C for (a) 30 min, (b) 60 min, (c) 90 min, form two hot spot zone and (d) 120 min, form one hot spot zone.

to 5 cm from the top surface. As a result, heat is dispersed to the top surface and the wall of the concrete, as shown in Fig. 20 (Case C). There was two hot spot zone in time 90 min in Fig. 20(c) and one hot spot zone at 120 min in Fig. 20(d).

The heat distribution at the concrete surface differs according to whether 800 W or 400 W of MW power are applied. The amount of electrical power used has a direct effect on the intensity of the electric field. In addition, the temperature increases as the curing increases. The maximum temperature in the concrete occurred at 3 to 5 cm from the top surface.

#### 5.2.6. Heating characteristics of a concrete workpiece subjected to MW energy

**5.2.6.1. Moisture Loss.** In this experiment, the water–cement ratio is 0.486 for all the studied cases. For the purpose of repairing concrete roads, the highway department sets a maximum limit on the water and cement (w/c) of 0.486 by mass. The water or moisture content in concrete means that concrete is a dielectric material capable of absorbing MW energy and transforming it into heat. Therefore, when concrete is energized by MW power, the moisture content of the concrete or the excess water from

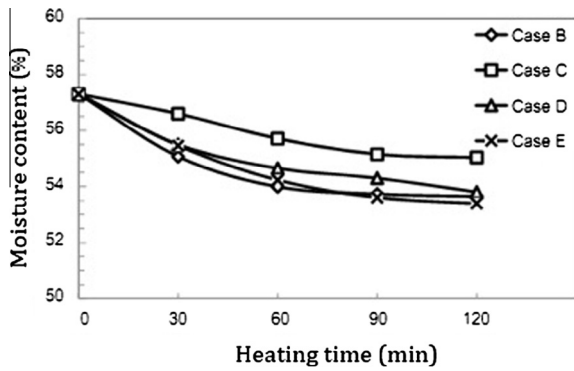


Fig. 21. Moisture content in concrete after MW curing in Cases B, C, D, and E.

hydration between the cement and water is reduced. In addition, the concrete is energized by continuous MW power, the moisture content decreases and thereby affects the moisture-transfer mechanism in the concrete (porous material theory).

The results pertaining to the amount of moisture lost from the concrete after MW curing in Cases B, C, D, and E are presented in Fig. 21. Overall, the moisture content of the concrete undergoes rapid changes at the beginning of the curing phase. The moisture distribution and porosity are related to many factors, i.e., the moisture content transfer from within the concrete to its surface, the changing state of fresh concrete from the liquid to gas phase, and the moisture transfer from the thermal distribution. At first, the moisture content at the surface of the concrete absorbs MW energy, which is then transformed into heat energy. The rate of evaporation is equal to the water movement in porous materials that creates the liquid film. The controlled parameter is the level of the heat energy input into the concrete. When the process whereby moisture is removed has been carried out, the internal moisture is reduced, and this reduced moisture content has a direct effect on the concrete's dielectric property. The moisture content is reduced, and the heat generation is reduced likewise (heat transfer and mass in porous material).

**5.2.6.2. Compressive strength development.** Compressive strength is the most important property of concrete. The main function of concrete is load resistance, which is a direct function of compressive strength. Further, compressive strength is an indicator of other important properties, namely, durability, friction resistance, and porosity resistance.

This research focuses on concrete with compressive strength of at least 325 kg/cm<sup>2</sup> for concrete at age 28 days. MW technology is applied in order to accelerate the curing time because a road repair carried out based on conventional curing can mean that a road is out of use for as many as 14 days. For this special case, compressive strength must be a minimum of 245 kg/cm<sup>2</sup>.

The experiment whereby concrete is cured using MW energy is divided into two parts: the conventional water-curing case (Case A), air curing and MW curing (Cases B, C, D, and E, respectively), and moving curing (Case F).

Fig. 22 presents water and air curing (Case A). The results indicate that the concrete's compressive strength increased rapidly in the first 3 days. The initial curing phase can increase this property of concrete. During the first 3 days, water curing and air curing show a similar level of efficiency. After that period, however, under water curing, the concrete's compressive strength increases continuously until the age of 28 days when the compressive strength is equal to 405.59 kg/m<sup>2</sup>. On the other hand, under air curing after the first 3 days, the concrete shows only a slight increase in compressive strength until the age of 28 days when the compressive

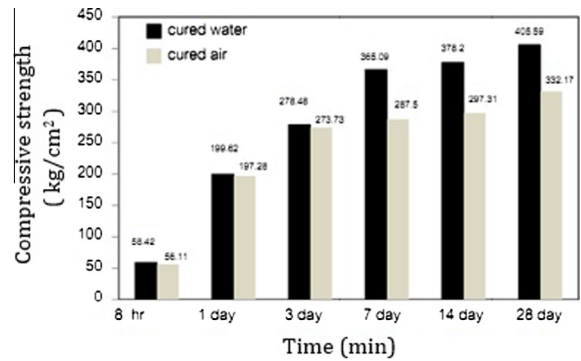


Fig. 22. Compressive strength of concrete after water and air curing (Case A).

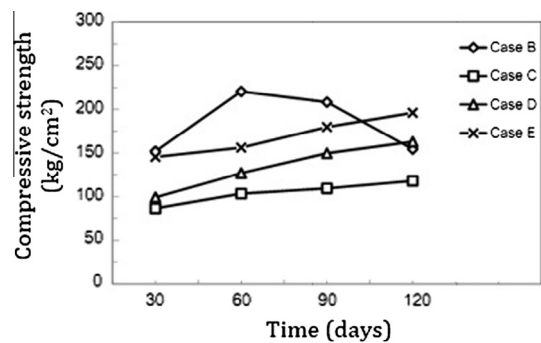


Fig. 23. Compressive strength of concrete after continuous MW curing and discontinuous MW curing for Cases B, C, D, and E.

strength is equal to 332.17 kg/cm<sup>2</sup>. The results show that water curing yields a higher level of compressive strength than air curing does. This is because under water curing, the moisture content facilitates the chemical reaction between cement and water, which serves to develop this concrete property.

Fig. 23 presents results pertaining to continuous MW curing and discontinuous MW curing for Cases B, C, D, and E. The results show that the compressive strength of the concrete as cured in Case B increased continuously at 30 and 60 min. Then, after 90 and 120 min, the compressive strength decreased continuously. Temperature has an effect on compressive strength development. In Case C, curing at 400 W, electrical power can continuously increase compressive strength. However, the compressive strength of the concrete in Case C increased slightly in comparison with the compressive strength of the concrete in Case B.

For Cases D and E, MW energizing was changed to a discontinuous mode and these two cases show the same level of compressive strength. The preheating together with the reduced idle time and reduced energized time are important factors in developing the concrete strength in Case D.

Fig. 24 presents the compressive strength of MW curing in the movement mode (Case F). The curing time is 18 h, 180 min of MW curing (not including idle time). The results indicate that the compressive strength levels of all six workpieces are similar. The average compressive strength is 193.45 kg/cm<sup>2</sup>. The speed of the motor for the movement study is 5 rpm with discontinuous MW energy applied. The PLC is applied in order to control horn movement.

The discontinuous MW curing used in Case E produces a high level of compressive strength when compared with the compressive strength developed in the Case C and Case D workpieces. Therefore, more experiments were performed. The curing time was extended by 60 min. Thus, the total time during which MW energy is applied for Case E is 180 min. The total time of this experiment is 13 h for MW curing.

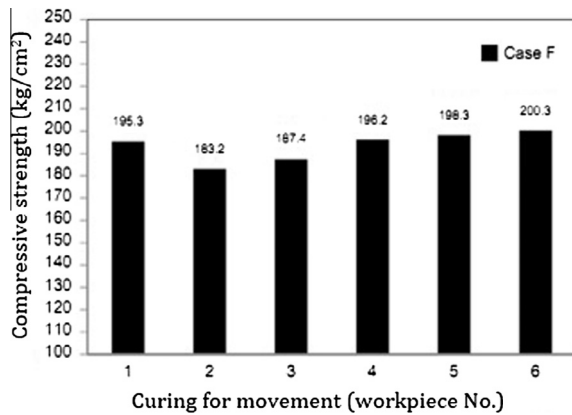


Fig. 24. The compressive strength of MW-cured concrete in the moving mode (Case F) at a curing time of 18 h and 180 min of MW curing (not including idle time).

The results show that compressive strength increases to 239 kg/cm<sup>2</sup> whereas moisture content after curing decreases to 53.3%. It can be concluded that this increased curing time can increase the compressive strength of the concrete and reduce its moisture content. However, the internal temperature is 113 °C, which should be studied in the future in order to determine the appropriate curing time and mixture design given the direct effects of water content in concrete on thermal distribution.

## 6. Conclusions and recommendation

In this research, MW-heating technology is applied in order to accelerate concrete curing. From the design and construction of a mobile MW-curing unit and an experimental investigation into the compressive strength of concrete dried using the prototype, the following conclusions can be drawn:

- The prototype design has many factors, i.e., the 1-axis movement and horn must be adjusted in a vertical direction [up-down], at 800 W power, and 2.45 GHz frequency.
- At the beginning of microwave curing, temperature of the concrete increased continuously. After 90 min, the temperature is constant because the moisture content at the surface of the concrete is reduced due to the absorption capacity of the MW energy.
- When concrete was heated using MW energy for more than 90 min at over 80 °C, the effect was a continuous decrease in compressive strength. Further, at early age, the compressive strength development of the concrete workpiece subjected to MW curing was greater than that achieved by air curing or water wet-curing.
- To produce maximum compressive strength, the appropriate preheating interval is 30 min combined with MW energizing for 15 min and a paused duration of 60 min.
- The highest strength achieved by MW curing is 239 kg/cm<sup>2</sup>, which is equal to 85% of the strength achieved by water curing. Thus, discontinuous MW curing for 120 min represents a significant reduction in curing time as compared with the time needed for water curing.
- In order to manage hot spots taking place during MW curing, moving cavity should be investigated in terms of moving speed, and temperature distribution from one specimen to the others.

## Acknowledgments

The authors gratefully acknowledge the Thailand Research Fund under the TRF contract Nos. RTA5680007 and TRG5780255, and

the National Research Universities Project of the Higher Education Commission for supporting this research.

## References

- [1] K.G. Ayappa, H.T. Davis, E.A. Davis, J. Gordon, Two dimensional finite element analysis of microwave heating, *AIChE J.* 38 (1992) 1577–1592.
- [2] C. Saliel, A. Datta, Heat and mass transfer in microwave processing, *Adv. Heat Transfer* 30 (1997) 1–94.
- [3] P. Heider, Computation of scattering resonances for dielectric resonators, *Int. J. Comput. Math. Appl.* 60 (2010) 1620–1632.
- [4] P. Chen, C.H. Wang, J.R. Ho, A lattice Boltzmann model for electromagnetic waves propagating in a one-dimensional dispersive medium, *Int. J. Comput. Math. Appl.* 65 (2013) 961–973.
- [5] M. Regier, H. Schubert, *Microwave processing*. In *The Microwave Processing of Foods*, Woodhead Publishing, Sawston, Cambridge, USA, 2001.
- [6] N. Afrin, Y. Zhang, J.K. Chen, Thermal lagging in living biological tissue based on non-equilibrium heat transfer between tissue, arterial and venous bloods, *Int. J. Heat Mass Transfer* 54 (2011) 2419–2426.
- [7] N. Irishina, O. Dorn, M. Moscoso, A level set evolution strategy in microwave imaging for early breast cancer detection, *Int. J. Comput. Math. Appl.* 56 (2008) 607–618.
- [8] T. Basak, Role of resonance on microwave heating of oil–water emulsions, *AIChE J.* 50 (2004) 2659–2675.
- [9] P. Perre, I.W. Turner, Microwave drying of softwood in an oversized waveguide: theory and experiment, *AIChE J.* 43 (10) (1997) 2579–2595.
- [10] W. Kaensup, S. Wongwiset, S. Chutima, Drying of pepper seeds using a combined microwave fluidized bed dryer, *Dryong Technol.* 16 (3–5) (1998) 853–862.
- [11] K.Y. Leung, T. Pheeraphan, Microwave curing of Portland cement concrete: experimental results and feasibility for practical applications, *Constr. Build. Mater.* (1995) 67–73.
- [12] N. Makul, P. Rattanadecho, D.K. Agrawal, Microwave curing at operating frequency of 2.45 GHz of Portland cement paste at early-stage using a multi-mode cavity: experimental and numerical analysis on heat transfer characteristics, *Int. J. Heat Mass Transfer* 37 (2010) 1487–1495.
- [13] American Concrete Institute, *ACI 318–Building Code Requirements for Structural Concrete and Commentary*, 2008. Farmington Hills, MI, USA.
- [14] P. Rattanadecho, N. Suwannapum, B. Chatveera, D. Atong, N. Makul, Development of compressive strength of cement paste under accelerated curing by using a continuous microwave thermal processor, *Mater. Sci. Eng. A* 472 (2008) 299–307.
- [15] W. Xuequan, Microwave curing technique in concrete manufacture, *Cem. Concr. Res.* 17 (2) (1987) 205–210.
- [16] R.G. Hutchison, Thermal acceleration of Portland cement mortars with microwave energy, *Cem. Concr. Res.* 21 (5) (1991) 795–799.
- [17] D. Sohn, D.L. Johnson, Microwave curing effect on the 28 day strength of cementitious materials, *Cem. Concr. Res.* 29 (1999) 241–247.
- [18] *Microwave Method and Apparatus for Heating Pavement*, by M.R. Jeppson, C. Calif, (1981). United States Patent, 425 2 487.
- [19] A.C. Metaxas, R.J. Meridith, *Industrial Microwave Heating*, Peter Peregrinus Ltd, London, 1983.
- [20] *Concrete Curing Machine*, by C.B. Sipherd, J.R. Lease, R.L. Stainbrook, (2002). United States Patent 649 7 531 B1.
- [21] T. Chow Ting Chan, H.C. Reader, *Understanding Microwave Heating Cavities*, Artech House Inc, Norwood, MA 02062 USA, 2000.
- [22] COMSOL Inc, *COMSOL Multiphysics User's Guide Version 3.4*, COMSOL AB, Singapore, 2007.
- [23] P. Rattanadecho, K. Aoki, M. Akahori, Experimental and numerical study of microwave drying in unsaturated porous material, *Int. J. Heat Mass Transfer* 28 (2001) 605–616.
- [24] S. Hauck Harold, Design considerations for microwave oven cavities, *IEEE Xplore: IEEE Transactions on Industry Applications* (1) (1970) 74–80. Vol. IGA-6.
- [25] L.A. Campanone, N.E. Zaritzky, Mathematical analysis of microwave heating process, *J. Food Eng.* 69 (2005) 359–368.
- [26] American Society for Testing and Materials, *ASTM C150-12 Standard Specification for Portland Cement*, Annual Book of ASTM Standards, 4.01, 2012. Philadelphia, PA, USA.
- [27] American Society for Testing and Materials, *ASTM C1602/C1602M - 12 Standard Specification for Mixing Water Used in the Production of Hydraulic Cement Concrete*, Annual Book of ASTM Standards, 4.02, 2012. Philadelphia, PA, USA.
- [28] American Society for Testing and Materials, *ASTM C33/C33M - 13 Standard Specification for Concrete Aggregates*, Annual Book of ASTM Standards, 4.02, 2013. Philadelphia, PA, USA.
- [29] British Standards Institution, *BS 1881: Part 3, Method of Making and Curing Test Specimens*, 2011. London, United Kingdom.
- [30] American Society for Testing and Materials, *ASTM C192/C192M-14 Standard Practice for Making and Curing Concrete Test Specimens in the Laboratory*, Annual Book of ASTM Standards, 4.02, 2014. Philadelphia, PA, USA.
- [31] British Standards Institution, *BS 1881: Part 4, Method of Testing Concrete for Strength*, 2011. London, United Kingdom.